10 YEARS ANNIVERSARY

INORGANIC
CHEMISTRY
FRONTIERS

Tera-hertz (THz) catalysis on MXene for enhanced selectivity from CO_2 to CO†

Ziao Wang,[a] Yao Xu,[a] Tao Feng,[b] Chaojun Lei,[b] Yu Zhao [iD] *[b] and Xi Zhu [iD] *[a]

Applying Natural Language Processing (NLP) to journals about catalytic reaction, we found a gap between photocatalysts and thermal catalysts, where Tera-Hertz (THz) catalysis is located; therefore, we have investigated THz catalysis in this work. We report an excellent $Ti_3C_2F_2$ MXene electrocatalyst that can accelerate the catalytic process of the hydrogen evolution reaction (HER) and carbon dioxide reduction reaction (CO_2RR). In the CO_2RR reaction, high selectivity toward the gaseous product CO is observed. The THz catalysis is achieved through the resonance between the vibrational mode of CO_2 and the surface phonon mode. Detailed computational studies are discussed. Potential applications of MXene in THz catalysis in the future are also expected.

Introduction

Natural language processing (NLP), one of the most promising AI technology fields, has been recommended to solve the literature-based knowledge transformation problem. Data mining and NLP technologies have recently allowed researchers to implement an automated extraction pipeline on unstructured scientific publications. Some of the most famous toolkits for literature collection and chemical entity recognition are CrossRef,[1] ChemDataExtractor,[2] ChemicalTagger,[3] *etc*. Most of the existing data extraction and data mining efforts have used modeling and machine learning to predict the structure–property relationships of materials.[4,5] Applying NLP to catalytic reactions, extracting the keywords of catalytic conditions, and arranging them according to the corresponding wavelengths of the reaction conditions, we found that there is a "gap" between photocatalysts and thermal catalysts, which corresponds to the wavelength range of Tera-Hertz (THz) catalysis, as shown in Fig. 1.

The direct application of THz in catalysis stems from the work of Jerry L. LaRue *et al.* (2015).[6] They presented evidence

[a]*School of Science and Engineering (SSE), Shenzhen Institute of Artificial Intelligence and Robotics for Society (AIRS), The Chinese University of Hong Kong, Shenzhen (CUHK-Shenzhen), Shenzhen, Guangdong, 518172, P. R. China.*
E-mail: zhuxi@cuhk.edu.cn
[b]*College of Material, Chemistry and Chemical Engineering, Key Laboratory of Organosilicon Chemistry and Material Technology, Ministry of Education, Hangzhou Normal University, Hangzhou, Zhejiang, 311121, P. R. China.*
E-mail: yuzhao@hznu.edu.cn
†Electronic supplementary information (ESI) available. See DOI: https://doi.org/10.1039/d2qi02476d

that CO oxidation on Ru(001) was selectively induced, rather than the promotion of the thermally-induced CO desorption process, using strong electric fields from THz pulses generated by coherent transition radiation from ultrashort electron beams. The reaction is triggered by the motion of O atoms on the surface driven by the electric field component of the THz pulse rather than the thermal heating of the surface. The application of THz in other catalytic processes is worthy of further exploration.

MXenes consist of layers of transition metal carbides, nitrides, or carbonitrides several atoms thick. The outstanding electrical conductivity and the hydrophilic surface of MXenes also ensure their usefulness in the hydrogen evolution reaction (HER),[7–9] oxygen evolution reaction (OER),[10–12] oxygen reduction reaction (ORR),[13,14] nitrogen reduction reaction (NRR)[15–17] and carbon dioxide reduction reaction (CO_2RR).[18] MXene has been proven to produce significant effects in the field of electrocatalysis. Due to the surface termination T_x (mainly fluorine, –F, oxygen, –O, and hydroxyl, –OH) groups, most MXenes show both metal conductivity and hydrophilicity.[19] Some recent reports have shown that MXenes could be used as excellent THz detection materials based on density functional theory (DFT) calculations.[20] Some subsequent works have taken advantage of this special property of MXenes for applications in different fields, such as using MXenes as THz absorbers,[21] the transformation of THz waves to heat,[22] and THz radiation shields.[23] These works show that MXene has better performance under THz irradiation than in the normal state, and the application of this combination in other fields deserves to be further developed.

In the reaction process of CO_2RR, two gaseous products, carbon monoxide (CO) and methane (CH_4), play a crucial
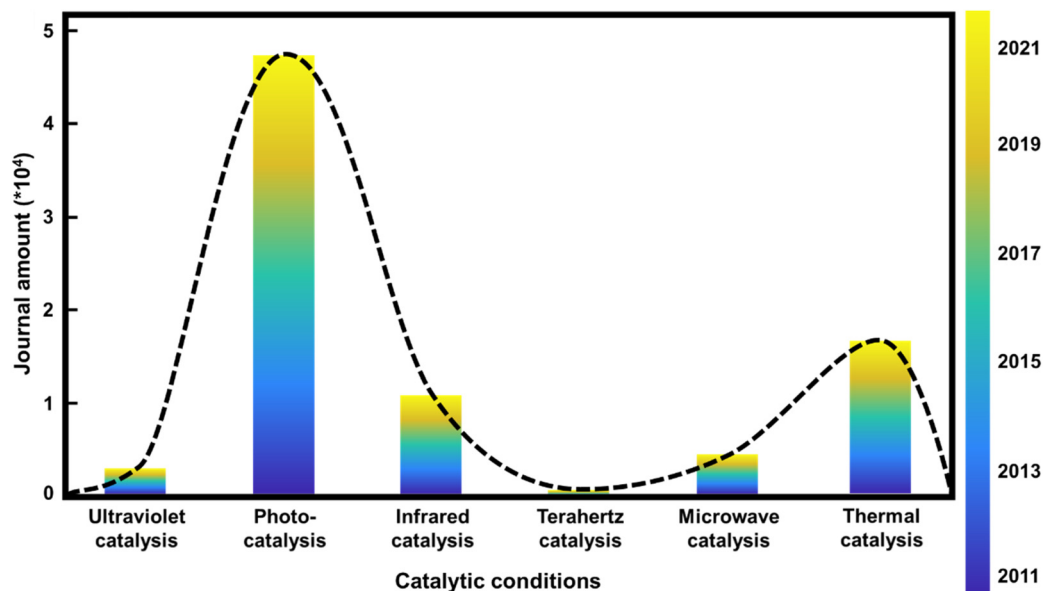
Fig. 1 Heat map of the NLP analysis of catalytic journals. The *x*-axis represents the catalytic conditions in the order of the corresponding wavelengths (from short to long wavelength). The *y*-axis represents the amount of journal reports for each condition. The color bar represents the publication years from bottom (blue) to top (yellow).

role. Since the two products are produced in different reaction steps in the same process and are difficult to separate, it is important to control the selectivity to obtain them separately. Most of the existing control methods for the selectivity of the two products involve performing secondary processing of the electrode to obtain a composite electrode to enhance the output of one of the products.[24,25] However, most electrode modification methods are too complex and expensive to enable many industrial applications and cannot be selectively replaced according to practical needs.

In this work, we were inspired to perform MXene electrochemical processes using THz catalysis by the analysis of about 79 500 NLP-processed articles. We designed an automated synthesis process for MXene and connected an *in situ* Raman apparatus and *in situ* gas chromatography (GC) test device to the electrolyzer to automate the reaction process and test the sample preparation process. With MXene as the electrode, the current intensity of the electrochemical processes of HER and CO_2RR becomes stronger under irradiation with THz waves. Especially in the CO_2RR process, the THz waves affect the selectivity of the gaseous products, carbon monoxide and methane. DFT calculations confirmed two things. One is that under the influence of THz irradiation, the free energy of the key steps of the two electrochemical processes becomes lower, which makes the electrochemical reaction more likely to occur, increasing current intensity. The other is that THz irradiation will affect the vibration of CO molecules on the surface of MXene, making the CO_2RR reaction more inclined to generate CO gas, the macroscopic manifestation of which is that the selectivity of the product has been enhanced.

Results and discussion

Our work is motivated by generalizing existing publications through NLP analysis. We integrate and classify the literature data according to the reaction conditions, arrange the reaction conditions in a certain order (the reaction conditions in this article are arranged by the corresponding wavelength range), and obtain a trend data map of the reaction conditions in catalytic reactions in recent years. The comparison of relevant factors of different keyword combinations is shown in Fig. 1. Compared to the more popular photocatalysis and thermal catalysis, research into catalysis using THz waves, which will be a new generation of communication signals widely used in daily life, is gradually arousing interest. The excited electrons drive the atoms to move in photo-catalysis, while the atoms' movements drive electrons to transfer in thermal catalysis. Therefore, with THz waves being in the middle of the wavelength ranges for these two catalytic conditions, THz irradiation can achieve better coupling of the promotion of atomic and electronic vibration and can further improve the efficiency of the reaction, which is worthy of further exploration. Additionally, MXene can absorb THz waves and show better performance and properties due to the intrinsic phonon spectrum. Therefore, the combination of MXene catalysts and THz catalytic conditions is the area that should be explored.

Single-layer Ti_3C_2Tx nanoflakes are generally synthesized by selectively etching the Al atoms from MAX precursor (Ti_3AlC_2) phases, followed by a delamination process.[26] Hydrofluoric acid (HF) is needed during the synthesis of MXene, which is synthesized from fluorite (calcium fluoride, CaF_2, for the main component). However, it is extremely corrosive and can cause incurable burns when the vapors are inhaled or come in

2904 | *Inorg. Chem. Front.*, 2023, **10**, 2903–2910

This journal is © the Partner Organisations 2023

contact with the skin. Therefore, a robotic arm was used to synthesize MXene to prevent danger to humans from the HF produced during the reaction.

A schematic and physical diagram of the synthesis process of MXene with the assistance of a robotic arm is shown in Fig. 2(a). The heating kettle used for the MXene synthesis reaction was prepared and moved using robotic arms for safety due to the HF that would be generated during the reaction. The kettle was moved to an automated liquid injection pump for the addition of liquid reactants. The heating kettle was then moved to the heating table accurately and gently placed on a customized metal heating platform matching its shape, and heating was initiated to proceed with the synthesis reaction. Upon completion of the reaction, an MXene solid would be formed. To separate the MXene product, we used a suction filter to achieve the separation. The heating kettle was slowly taken from the heating platform and moved to the side of the suction filter device. The wrist of the robotic arm was turned to pour the liquid, and the suction filter process was automati-

cally started. The heating kettle was kept in the pouring state for a while to ensure that all materials were poured out. Since the device was specifically used to recycle the synthesis reaction of MXene, the next cycle of the MXene synthesis experiment could be started without special cleaning.

By using the robotic arm to move the reaction vessel, inject the raw reaction materials, and directly post-process the products, the experimenters avoid exposure to the extremely corrosive materials that may appear during the reaction, such as hydrofluoric acid, *etc.*, ensuring the safety of the entire experiment. At the same time, because the device can automatically fill the reactants, we only need to prepare many reactants to keep the device reacting, reducing unnecessary experimental operations and improving production efficiency.

To explore the performance changes of the MXenes under THz irradiation, we employed *in situ* Raman testing techniques. The device arrangement is shown in Fig. 2(b). We used an electrolytic cell with mirrors, ensuring that Raman spectroscopy testing and data collection were carried out simul-
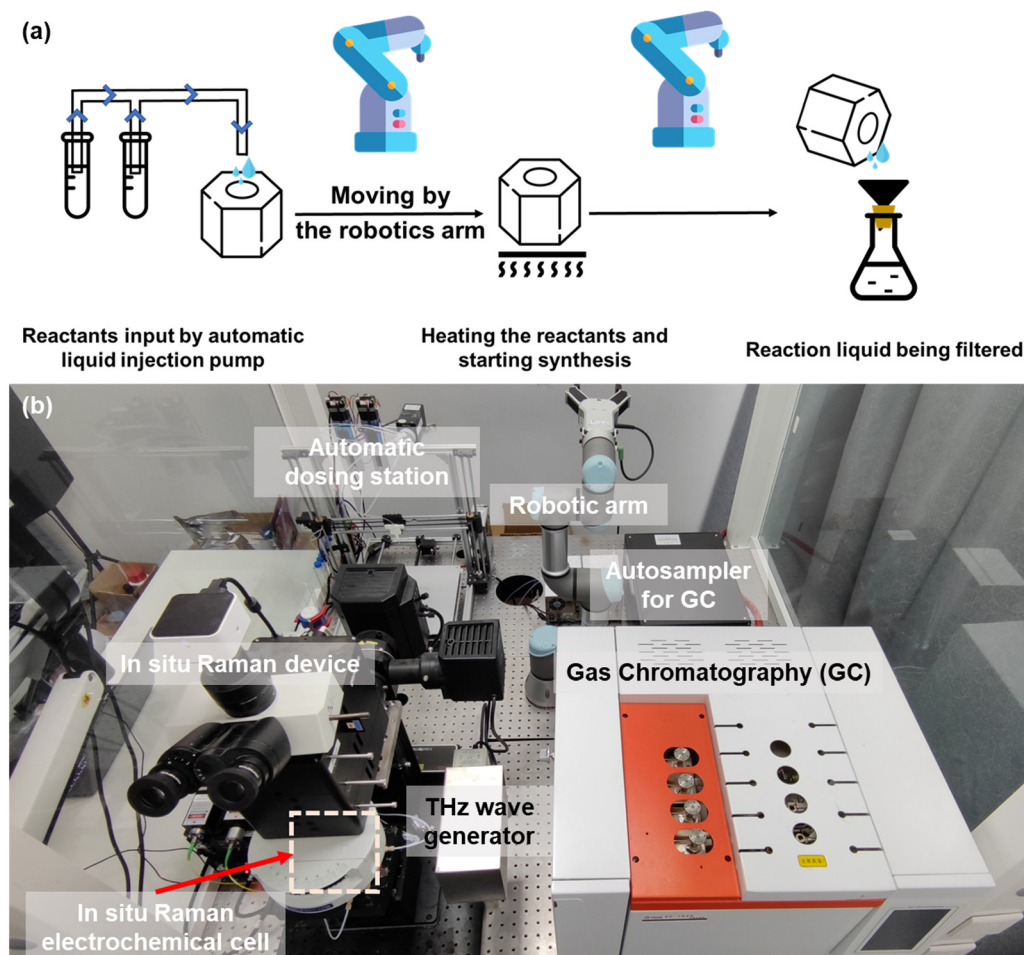

Fig. 2 (a) Schematic diagram of the robotic-arm-assisted automated MXene synthesis process. Robotic arms moved the heating kettle for safety due to the HF generated during the process. (b) Physical map of the robotic-arm-assisted electrolyte preparation device, electrocatalytic reaction device (*in situ* Raman electrochemical cell), and *in situ* Raman and GC test setup. The THz wave generator was a model CQ-8 THz electromagnetic wave therapy device.[27]

This journal is © the Partner Organisations 2023

Inorg. Chem. Front., 2023, **10**, 2903–2910 | **2905**

taneously with electrochemical catalytic testing. A THz wave generator was set beside the electrochemical cell for the THz irradiation experiment. The THz wave was from a model CQ-8 THz electromagnetic wave therapy device,[27] whose frequency range is from 3 to 15 THz. There was a 1 cm × 1 cm opening in the middle of the container, which precisely controlled the effective reaction area of the electrode and facilitated the analysis and processing of subsequent data. On the other hand, when conducting CO_2RR experiments, the product must be analyzed using gas chromatography to confirm the chemical components in the product and compare the production amounts. We connected the gas output of the electrolyzer and the gas input of the gas chromatography directly and used the autosampler to collect the product gas and feed the gas chromatograph, isolating the product gas from the outside world to ensure the accuracy of the test.

Scanning electronic microscopy (SEM) images of the automatically synthesized MXene fragments and enlarged regions of them are shown in ESI Fig. S1(a) and (b).† The 2D structure of MXene was clearly observed after the automatic synthesis, which partially demonstrated the feasibility of MXene automatic synthesis. In the XRD data, the appearance of characteristic peaks also indicates the structural integrity of the auto-synthesized MXenes (ESI Fig. S2†). To gain more information about the MXene surface chemistry, we performed an XPS analysis, and the results are shown in ESI Fig. S3.† The investigation showed clear signals from the elements Ti, C, O, and F. Specifically, peaks with binding energy values of 284 eV, 453 eV, 476 eV, 530 eV, 557 eV, and 682 eV were assigned to C 1s, Ti 2p, Ti $2p_{1/2}$, O 1s, Ti 2s, and F 1s, respectively, which were in good agreement with the EDAX results. The high-resolution XPS spectrum of the C 1s region of the MXene powders shows three main peaks at 281.4, 284.6, and 287.8 eV, probably from Ti–C, C–C, and C–O, respectively. The presence of C–O may come from MXene oxidation, leading to TiO_2 and carbon atomic network formation.

The device for the HER electrocatalysis experiment is shown in Fig. 3(a). The working electrode is carbon paper coated with an MXene layer, with a size of 1 cm × 1 cm. The electrocatalytic activity of the $Ti_3C_2F_2$ MXene was investigated for the HER in a 0.5 M H_2SO_4 solution. A THz generator was placed next to the electrolyte device for THz illumination, simulating the situation of collecting redundant THz waves in space. The linear sweep voltammetry (LSV) polarization curves of bare carbon paper (CP), bare MXene, MXene under heating, and MXene under THz irradiation were measured over a wide potential range from 0 to −0.6 V *vs.* RHE, as shown in Fig. 3(b). The heated solution environment and irradiation of the electrolytic cell with THz resulted in higher current densities than those of the bare MXene electrodes. The MXene under heating was more active in the HER process, achieving 7.3 mA cm^{-2} at an initial overpotential of 600 mV. THz irradiation can enable further activation of the MXene material electrodes. 10 mA cm^{-2} at an overpotential of 493 mV was achieved with an MXene catalyst under THz irradiation. The Tafel slope reflects the reaction kinetics of the hydrogen evol-

ution process. A lower Tafel slope indicates a faster reaction rate. Using the Tafel equation, the polarization curve yields a Tafel plot: $\eta = a + b \log j$, where η is the overpotential, a is the y-intercept, b is the Tafel slope, and j is the current density. As shown in Fig. 3(c), MXene under THz irradiation exhibits a lower Tafel slope of 115 mV dec^{-1} compared to the Tafel slope of CP (385 mV dec^{-1}), bare MXene (209 mV dec^{-1}) and MXene under heating (117 mV dec^{-1}), revealing the rapid HER kinetics derived from the THz irradiation.

Fig. S4† shows the electrochemical impedance spectra (EIS) of CP, bare MXene, MXene under heating, and MXene under THz irradiation. The charge transfer resistance of the MXene under THz irradiation is lower than that of CP, bare MXene, and MXene under heating, indicating a fast faradaic process and superior HER kinetics for the MXene under THz irradiation. To gain more insight into the enhanced HER performance, we calculated the double-layer capacitance (C_{dl}) of the catalysts from the CV measurements obtained in 0.5 M H_2SO_4. Fig. S5a† depicts the CV curves of the CP at different scan rates ranging from 5 to 60 mV s^{-1}. Similarly, the CV curves of MXene at different scan rates are shown in Fig. S5b.† We determined the C_{dl} value of the MXene to be 11.6 mF cm^{-2}, which is ≈12.6 times higher than that of the CP (0.92 mF cm^{-2}), as shown in Fig. 3(d), indicating the high electrochemically active area with exposed catalytic active sites available on MXene, which is favorable for boosting its HER performance.

Theoretical calculations of key steps in the HER process, which are shown in Fig. 3(e) and (f), demonstrated that THz promotes the electrocatalytic reaction of the MXene catalysts. Two models were calculated, $Ti_3C_2F_2$ MXene and $Ti_3C_2(OH)_2$ MXene. The HER on $Ti_3C_2F_2$ MXene under THz irradiation shows a smaller ΔG_H of 0.38 eV, which explains its higher HER activity compared to that of bare MXene, which has a calculated ΔG_H of 0.45 eV. Additionally, the HER on $Ti_3C_2(OH)_2$ MXene under THz irradiation shows a smaller ΔG_H of 0.40 eV. This result predicts its higher HER activity compared to that of bare MXene.

After determining the promoting effect of THz on the current intensity of MXene electrodes in the HER, we proceeded to investigate its CO_2RR catalytic activity. The device for the CO_2RR electrocatalysis experiment is shown in Fig. 4(a). The working electrode was carbon paper coated with an MXene layer, with a size of 1 cm × 1 cm. The electrocatalytic activity of the $Ti_3C_2F_2$ MXene was investigated for the CO_2RR in a 0.5 M $KHCO_3$ solution. The THz generator was placed next to the electrolyte device for THz irradiation, simulating the situation of collecting redundant THz waves in space. Linear sweep voltammetry (LSV) polarization curves of bare MXene, MXene under heating, and MXene under THz irradiation were measured under flowing CO_2 gas over a wide potential range from 0 to −1.25 V *vs.* RHE, as shown in Fig. 4(b). Irradiating the electrolytic cell with THz waves resulted in higher current densities than those achieved using bare MXene electrodes. Bare MXene and MXene under heating show no measurable activity within the potential window of interest. However, THz
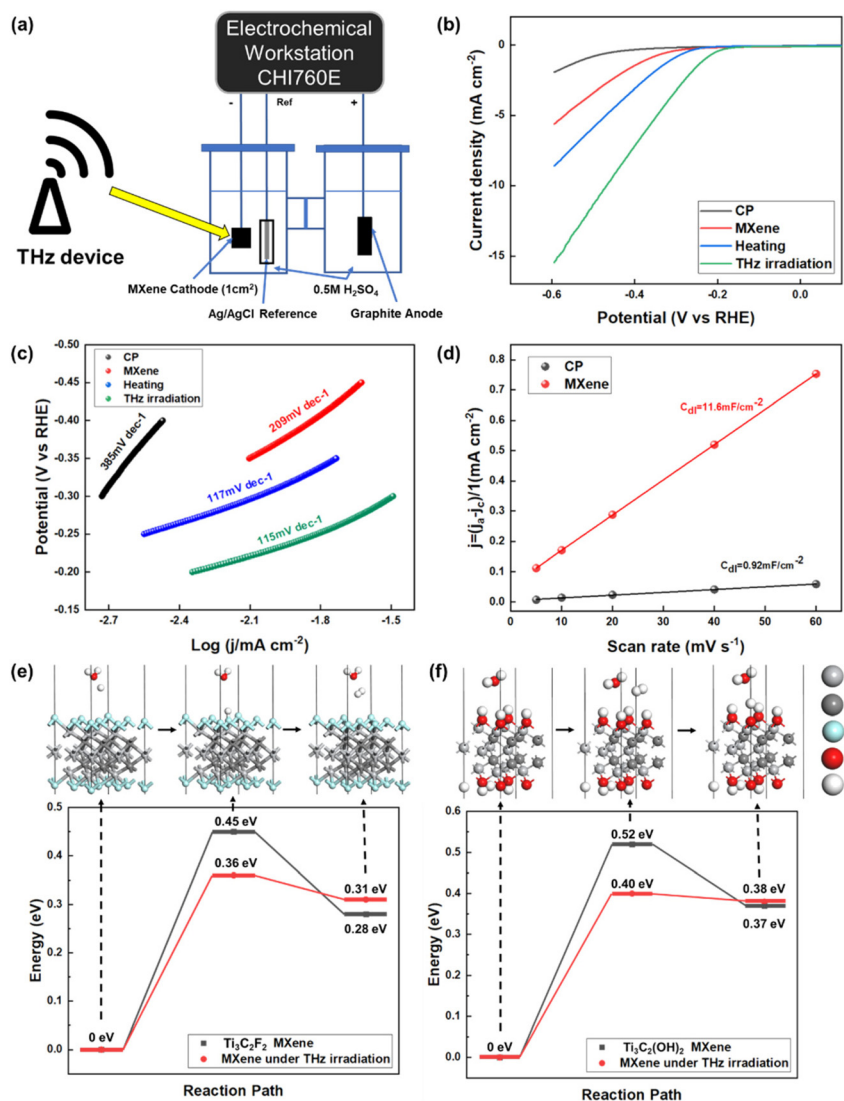
Fig. 3 (a) Schematic diagram of the HER electrocatalysis experiment. MXene was used as an electrode for electrocatalytic testing under THz irradiation. (b) LSV polarization curves and (c) Tafel plots of bare carbon paper (CP), bare MXene, MXene under heating, and MXene under THz irradiation. (d) Current density difference ($\Delta j = j_a - j_c$) plots of CP and MXene electrocatalysts at 0.455 V *versus* RHE as a function of scan rate, which were used to calculate the double-layer capacitance value (C_{dl}). DFT calculation of the free energy in (e) the HER process on the $Ti_3C_2F_2$ MXene surface and (f) the HER process on $Ti_3C_2(OH)_2$.

irradiation can enable further activation of MXene material electrodes. 10 mA cm^{-2} at an overpotential of 557 mV was achieved with the MXene catalyst under THz irradiation, as shown in Fig. 4(c). The generated current intensities of the materials were significantly different in the tested voltage range. MXene under THz irradiation achieved a current density of over 25 mA cm^{-2}, which was much larger than that of bare MXene and MXene under heating, as shown in Fig. 4(d). Different CO_2 gas flow rates had very little effect on the current intensity, which may be caused by the different effective areas of carbon dioxide contacting the electrode at different flow rates.

In the reaction process of CO_2RR, two gaseous products, carbon monoxide (CO) and methane (CH_4), play a crucial role. CO plays an essential role in producing many compounds,

including medicines, fragrances, and fuels. Methane is widely used as a fuel due to its high calorific value. Since the two products are produced in different reaction steps in the same process and are difficult to separate, it is important to control the selectivity to obtain them separately. Most of the existing methods for the control of the selectivity of the two products involve performing secondary processing of the MXene electrode to obtain a composite electrode to enhance the output of one of the products.[24] However, most electrode modification methods are too complex and expensive to enable many industrial applications, and cannot be selectively replaced according to practical needs.

In this work, we found that THz irradiation significantly affects the selectivity of the gaseous products in the electrocatalytic CO_2 reduction reaction. Compared to previous studies
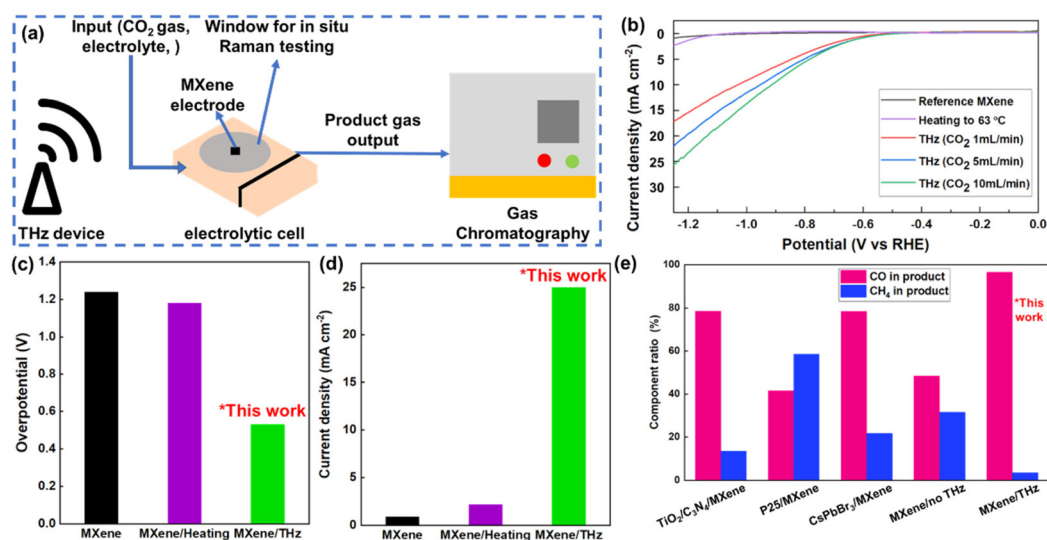
This journal is © the Partner Organisations 2023

Inorg. Chem. Front., 2023, **10**, 2903–2910 | **2907**

Fig. 4   (a) Schematic diagram of the *in situ* Raman testing and gas chromatography composition detection device. (b) LSV test of the CO_2RR under THz irradiation with different CO_2 input rates, heating to 70 °C, and reference conditions. (c and d) Overpotential difference and current density difference at −1.25 V of the CO_2RR under THz irradiation, heating, and reference conditions. (e) Selectivity comparison of CO and CH_4 yields in the products of the CO_2RR process under different MXene treatments, with the first three sets of data cited from previous literature data and the last two sets from our experiments under two conditions, which are MXene electrodes without and with THz wave irradiation.[19,23,29]

on gas product selectivity (Fig. 4(e)),[24,28] under THz irradiation, MXene exhibits greater propensity toward CO gas production. In the absence of THz irradiation, carbon monoxide and methane accounted for 48% and 31% of the total gas

product, respectively (the remainder being unreacted carbon dioxide gas). The addition of THz irradiation changes the proportions of the two gas products to 96% and 3%, respectively (comparison of the gas chromatograms for the gaseous pro-
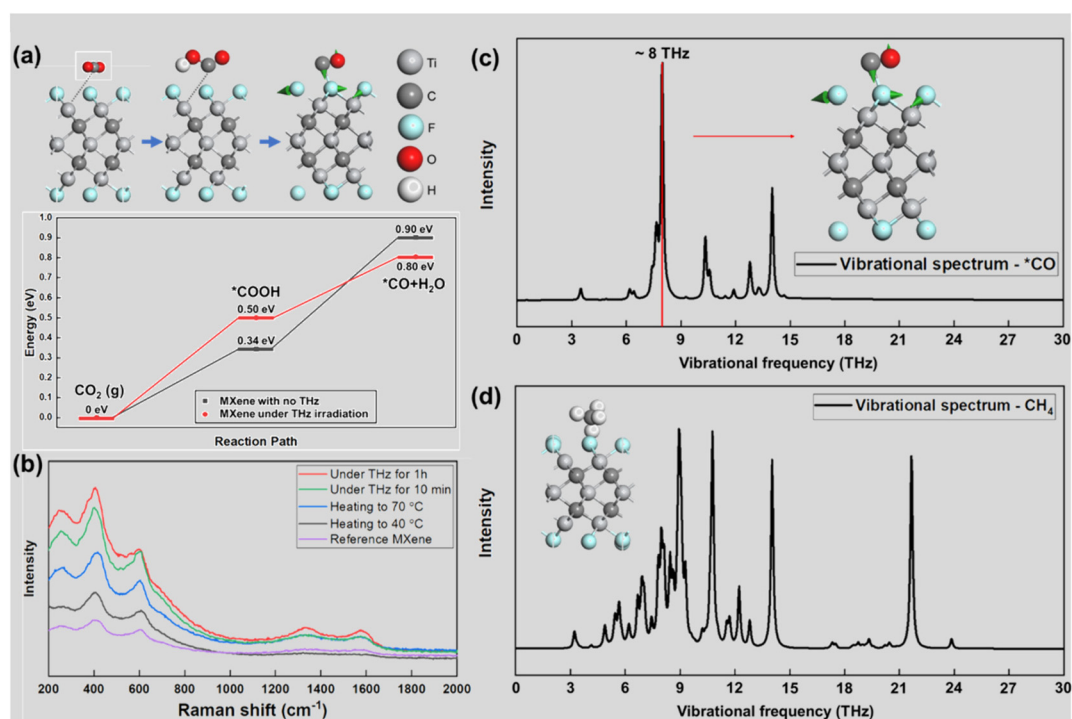

Fig. 5   (a) DFT calculation of the free energy in the CO_2RR process from CO_2 gas to *CO on the MXene surface. (b) Raman data of reference MXene, heated MXene, and MXene under THz irradiation. (c and d) Vibrational mode comparison of CO and CH_4 on the $Ti_3C_2F_2$ MXene surface; the highlighted peak in the vibrational spectrum of CO is located in the frequency range of the THz band (0.1–10 THz).

ducts of the electrochemical CO_2RR process under different conditions is provided in ESI Fig. S6†). This indicates that THz irradiation positively affects the reaction rate and efficiency of the CO_2 reduction reaction and decisively improves the selectivity toward CO.

Theoretical calculations on the key steps in the CO_2RR process, which are shown in Fig. 5(a) (structural diagrams of each key step are shown in ESI Fig. S7–S10†), demonstrate that THz irradiation promotes the electrocatalytic reaction of the MXene catalysts. The CO_2RR on $Ti_3C_2F_2$ MXene under THz irradiation shows a smaller ΔG_H of 0.80 eV, which explains its higher CO_2RR activity compared to that of bare MXene, which has a calculated ΔG_H of 0.90 eV. This demonstrates the positive effect of THz on the CO_2RR process. To explore the principle of the effect of THz irradiation on the gas products, we used the *in-situ* Raman testing technique to conduct real-time Raman spectroscopy observation; the spectrum data is presented in Fig. 5(b). The chemical bond vibration in MXene is continuously enhanced with the change in the external conditions from bare MXene to heating and THz irradiation. The increasing intensity of the peak at about 600 cm^{-1}, which is the peak position of *CO, indicates the increasing catalytic activity moving from normal conditions to THz irradiation. The theoretical calculations of the vibrational modes of the two gases on the MXene surface were also confirmed to match the previous experimental data. Two vibrational modes, those of CO and CH_4 on the MXene surface, are shown in Fig. 5(c) and (d). In the high-brightness range, in the THz band, CO has a single strong peak on the surface of MXene, and the vibrational mode shows that the vibration of the surface atoms resonates with that of CO molecules. This vibration enhancement causes the CO molecules to detach from the surface. On the contrary, methane molecules have no characteristic peaks in this band. There is little vibrational resonance between the methane and the surface modes of MXene, so the proportion of methane gas in the product will be reduced relative to that of carbon monoxide.

Conclusion

In summary, NLP indicates that THz catalysis is worthy of further exploration, and the combination of MXene and THz shows excellent HER and CO_2RR catalysis efficiency improvements. Automated processes were employed to help us with MXene synthesis and characterization. When MXene was used as an electrode and placed in an environment irradiated by THz waves for electrocatalytic testing, the results showed that MXene positively affected the HER and CO_2RR processes. Since the vibrational mode frequencies of Ti, C, and O in MXene are just within the THz range, MXene can absorb THz waves to produce a catalytic effect. Through calculations, it was found to positively catalyze the reduction process of carbon dioxide and reduce the activation energy of the reaction. THz irradiation will spread across all regions as new communication signals approach, and this discovery using MXene will have a wider range of application scenarios.

Conflicts of interest

There are no conflicts to declare.

Acknowledgements

References

1 R. Lammey, CrossRef text and data mining services, *Sci. Ed.*, 2015, **2**(1), 22–27.

2 M. C. Swain and J. M. Cole, ChemDataExtractor: a toolkit for automated extraction of chemical information from the scientific literature, *J. Chem. Inf. Model.*, 2016, **56**(10), 1894–1904.

3 L. Hawizy, D. M. Jessop, N. Adams and P. Murray-Rust, ChemicalTagger: A tool for semantic text-mining in chemistry, *J. Cheminf.*, 2011, **3**(1), 17.

4 G. Hautier, C. C. Fischer, A. Jain, T. Mueller and G. Ceder, Finding Nature's Missing Ternary Oxide Compounds Using Machine Learning and Density Functional Theory, *Chem. Mater.*, 2010, **22**(12), 3762–3767.

5 S. Curtarolo, G. L. W. Hart, M. B. Nardelli, N. Mingo, S. Sanvito and O. Levy, The high-throughput highway to computational materials design, *Nat. Mater.*, 2013, **12**(3), 191–201.

6 J. L. LaRue, T. Katayama, A. Lindenberg, A. S. Fisher, H. Ostrom, A. Nilsson and H. Ogasawara, THz-Pulse-Induced Selective Catalytic CO Oxidation on Ru, *Phys. Rev. Lett.*, 2015, **115**(3), 036103.

7 Z. P. Lv, W. S. Ma, M. Wang, J. Dang, K. L. Jian, D. Liu and D. J. Huang, Co-Constructing Interfaces of Multiheterostructure on MXene ($Ti_3C_2T_x$)-Modified 3D Self-Supporting Electrode for Ultraefficient Electrocatalytic HER in Alkaline Media, *Adv. Funct. Mater.*, 2021, **31**(29), 2102576.

8 Z. W. Seh, K. D. Fredrickson, B. Anasori, J. Kibsgaard, A. L. Strickler, M. R. Lukatskaya, Y. Gogotsi, T. F. Jaramillo and A. Vojvodic, Two-Dimensional Molybdenum Carbide (MXene) as an Efficient Electrocatalyst for Hydrogen Evolution, *ACS Energy Lett.*, 2016, **1**(3), 589–594.

9 C. Cui, R. F. Cheng, H. Zhang, C. Zhang, Y. H. Ma, C. Shi, B. B. Fan, H. L. Wang and X. H. Wang, Ultrastable MXene@Pt/SWCNTs' Nanocatalysts for Hydrogen Evolution Reaction, *Adv. Funct. Mater.*, 2020, **30**(47), 2000693.

10 M. Z. Yu, S. Zhou, Z. Y. Wang, J. J. Zhao and J. S. Qiu, Boosting electrocatalytic oxygen evolution by synergistically

This journal is © the Partner Organisations 2023

Inorg. Chem. Front., 2023, **10**, 2903–2910 | **2909**

coupling layered double hydroxide with MXene, *Nano Energy*, 2018, **44**, 181–190.

11 L. Y. Xiu, Z. Y. Wang, M. Z. Yu, X. H. Wu and J. S. Qiu, Aggregation-Resistant 3D MXene-Based Architecture as Efficient Bifunctional Electrocatalyst for Overall Water Splitting, *ACS Nano*, 2018, **12**(8), 8017–8028.

12 J. X. Chen, Q. W. Long, K. Xiao, T. Ouyang, N. Li, S. Y. Ye and Z. Q. Liu, Vertically-interlaced NiFeP/MXene electrocatalyst with tunable electronic structure for high-efficiency oxygen evolution reaction, *Sci. Bull.*, 2021, **66**(11), 1063–1072.

13 Z. Li, Z. Zhuang, F. Lv, H. Zhu, L. Zhou, M. Luo, J. Zhu, Z. Lang, S. Feng, W. Chen, L. Mai and S. Guo, The Marriage of the FeN$_4$ Moiety and MXene Boosts Oxygen Reduction Catalysis: Fe 3d Electron Delocalization Matters, *Adv. Mater.*, 2018, **30**(43), e1803220.

14 J. N. Chen, X. L. Yuan, F. L. Lyu, Q. X. Zhong, H. C. Hu, Q. Pan and Q. Zhang, Integrating MXene nanosheets with cobalt-tipped carbon nanotubes for an efficient oxygen reduction reaction, *J. Mater. Chem. A*, 2019, **7**(3), 1281–1286.

15 Y. Luo, G.-F. Chen, L. Ding, X. Chen, L.-X. Ding and H. Wang, Efficient electrocatalytic N$_2$ fixation with MXene under ambient conditions, *Joule*, 2019, **3**(1), 279–289.

16 L. Li, X. Y. Wang, H. R. Guo, G. Yao, H. B. Yu, Z. Q. Tian, B. H. Li and L. Chen, Theoretical Screening of Single Transition Metal Atoms Embedded in MXene Defects as Superior Electrocatalyst of Nitrogen Reduction Reaction, *Small Methods*, 2019, **3**(11), 1900337.

17 Y. Fang, Z. Liu, J. Han, Z. Jin, Y. Han, F. Wang, Y. Niu, Y. Wu and Y. Xu, High-Performance electrocatalytic conversion of N$_2$ to NH$_3$ using oxygen-vacancy-rich TiO$_2$ in situ grown on Ti$_3$C$_2$T$_x$ MXene, *Adv. Energy Mater.*, 2019, **9**(16), 1803406.

18 T. P. Nguyen, D. M. T. Nguyen, D. L. Tran, H. K. Le, D. V. N. Vo, S. S. Lam, R. S. Varma, M. Shokouhimehr, C. C. Nguyen and Q. V. Le, MXenes: Applications in electrocatalytic, photocatalytic hydrogen evolution reaction and CO$_2$ reduction, *Mol. Catal.*, 2020, **486**, 110850.

19 M. Naguib, O. Mashtalir, J. Carle, V. Presser, J. Lu, L. Hultman, Y. Gogotsi and M. W. Barsoum, Two-dimensional transition metal carbides, *ACS Nano*, 2012, **6**(2), 1322–1331.

20 Y. I. Jhon, M. Seo and Y. M. Jhon, First-principles study of a MXene terahertz detector, *Nanoscale*, 2018, **10**(1), 69–75.

21 W. Shui, J. Li, H. Wang, Y. Xing, Y. Li, Q. Yang, X. Xiao, Q. Wen and H. Zhang, Ti$_3$C$_2$T$_x$ MXene sponge composite as broadband terahertz absorber, *Adv. Opt. Mater.*, 2020, **8**(21), 2001120.

22 R. Li, L. Zhang, L. Shi and P. Wang, MXene Ti$_3$C$_2$: An Effective 2D Light-to-Heat Conversion Material, *ACS Nano*, 2017, **11**(4), 3752–3759.

23 Q. Zou, W. Guo, L. Zhang, L. Yang, Z. Zhao, F. Liu, X. Ye, Y. Zhang and W. Shi, MXene-based ultra-thin film for terahertz radiation shielding, *Nanotechnology*, 2020, **31**(50), 505710.

24 M. Ye, X. Wang, E. Liu, J. Ye and D. Wang, Boosting the Photocatalytic Activity of P25 for Carbon Dioxide Reduction by using a Surface-Alkalinized Titanium Carbide MXene as Cocatalyst, *ChemSusChem*, 2018, **11**(10), 1606–1611.

25 H. Lv, F. Lv, H. Qin, X. Min, L. Sun, N. Han, D. Xu, Y. Li and B. Liu, Single-Crystalline Mesoporous Palladium and Palladium-Copper Nanocubes for Highly Efficient Electrochemical CO$_2$ Reduction, *CCS Chem.*, 2022, **4**(4), 1376–1385.

26 J. Tang, T. Mathis, X. Zhong, X. Xiao, H. Wang, M. Anayee, F. Pan, B. Xu and Y. Gogotsi, Optimizing ion pathway in titanium carbide MXene for practical high-rate supercapacitor, *Adv. Energy Mater.*, 2021, **11**(4), 2003025.

27 ChongQing Aerospace Launch Vehicle Electronic Technology Co., Ltd, **https://www.cqhtyl.com**.

28 A. Pan, X. Ma, S. Huang, Y. Wu, M. Jia, Y. Shi, Y. Liu, P. Wangyang, L. He and Y. Liu, CsPbBr$_3$ Perovskite Nanocrystal Grown on MXene Nanosheets for Enhanced Photoelectric Detection and Photocatalytic CO$_2$ Reduction, *J. Phys. Chem. Lett.*, 2019, **10**(21), 6590–6597.

29 C. Chaccour, M. N. Soorki, W. Saad, M. Bennis, P. Popovski and M. Debbah, Seven defining features of terahertz (THz) wireless systems: A fellowship of communication and sensing, *IEEE Commun. Surv. Tutor.*, 2022, **24**(2), 967–993.

2910 | *Inorg. Chem. Front.*, 2023, **10**, 2903–2910

This journal is © the Partner Organisations 2023